nature materials

ARTICLES

PUBLISHED ONLINE: 3 AUGUST 2014 | DOI: 10.1038/NMAT4039

# Dynamic layer rearrangement during growth of layered oxide films by molecular beam epitaxy

J. H. Lee[1†‡], G. Luo[2‡], I. C. Tung[1,3], S. H. Chang[4], Z. Luo[4,5], M. Malshe[6], M. Gadre[2], A. Bhattacharya[4,7], S. M. Nakhmanson[8], J. A. Eastman[4], H. Hong[1], J. Jellinek[6], D. Morgan[2*], D. D. Fong[4] and J. W. Freeland[1*]

**The $A_{n+1}B_nO_{3n+1}$ Ruddlesden–Popper homologous series offers a wide variety of functionalities including dielectric, ferroelectric, magnetic and catalytic properties. Unfortunately, the synthesis of such layered oxides has been a major challenge owing to the occurrence of growth defects that result in poor materials behaviour in the higher-order members. To understand the fundamental physics of layered oxide growth, we have developed an oxide molecular beam epitaxy system with *in situ* synchrotron X-ray scattering capability. We present results demonstrating that layered oxide films can dynamically rearrange during growth, leading to structures that are highly unexpected on the basis of the intended layer sequencing. Theoretical calculations indicate that rearrangement can occur in many layered oxide systems and suggest a general approach that may be essential for the construction of metastable Ruddlesden–Popper phases. We demonstrate the utility of the new-found growth strategy by performing the first atomically controlled synthesis of single-crystalline $La_3Ni_2O_7$.**

The atomic-level synthesis of functional oxides and an understanding of their growth behaviour provide opportunities to explore and control the intriguing properties of artificial layered oxide heterostructures[1–3]. Oxide molecular beam epitaxy (MBE) has long been known to be a technique uniquely suited to the deposition of layered oxide materials that cannot be stabilized in bulk form[4–6], as the shuttered deposition process permits the construction of a material atomic layer by atomic layer. However, the desire for high crystal quality requires sufficient adatom mobility to achieve the two-dimensional growth mode, where each layer is completed before the next layer begins. With the elevated temperatures necessary for this mobility, other kinetic pathways (or other phases) may become competitive, and the resulting structure will be dictated by local thermodynamic and kinetic considerations[7].

A long-standing challenge in the oxide thin-film community has been the growth of $(AO)(ABO_3)_n$ Ruddlesden–Popper compounds[8], which consist of $n$ unit cells of perovskite $ABO_3$ alternated with a layer of rocksalt AO along the crystallographic $c$ axis. As an illustration of the utility of oxide MBE for the synthesis of layered phases, ref. 9 reported the growth of the first five members of the $(SrO)(SrTiO_3)_n$ homologous series ($n = 1$–5), and ref. 10 recently demonstrated the growth of a structure with $n = 10$. However, only a few members of the series are thermodynamically stable[11–13]. For this reason, as well as the high sensitivity of the material to the local Sr concentration, the resulting structures often exhibit intergrowth defects[14–16]. This highlights a clear need to quantitatively understand the interrelationships between the deposition process and naturally driven processes occurring within the growing crystal such that artificially layered structures can be more readily synthesized.

Here, we describe the results of a detailed study conducted on the initial growth of $Sr_2TiO_4$ ($n = 1$) on $TiO_2$-terminated $SrTiO_3$ (001) substrates[17,18], finding that the initial layers reconstruct through layer exchange into $SrTiO_3$ ($n = \infty$). The reaction can be understood from the energetics of different layer configurations determined with computational theory, and insight from these calculations is used to form the $Sr_2TiO_4$ phase directly by modification of the initial layering sequence. We then show the generality of the layer exchange phenomenon and demonstrate the utility of our growth strategy by stabilizing a new single-crystalline phase in the lanthanum nickelate system.

We employed a newly constructed oxide MBE system, built from an existing *in situ* X-ray chamber at Sector 33ID-E of the Advanced Photon Source[19] (APS). The $(SrO)(SrTiO_3)_n$ films were grown at 750 °C and in $10^{-6}$ Torr of $O_2$ using a Sr effusion cell and a Ti-Ball source. Immediately following the shuttered deposition of each atomic layer, with the sequence SrO → SrO → $TiO_2$ → SrO, we measured the scattered intensity under growth conditions along the out-of-plane direction (00$L$) at both non-resonant (15 keV) and resonant (at the Sr $K$-edge) X-ray energies. The X-ray results are shown in Fig. 1a, and the expected structure is shown in Fig. 1b. It can be readily observed that the intensity profile along the 00$L$, that is, the specular crystal truncation rod (CTR), for SrO no. 3 is virtually identical to that for SrO no. 2, which corresponds to the structure of a double SrO layer on the $SrTiO_3$ substrate. If the CTR for SrO no. 3 represents the same structure, this suggests that the $TiO_2$ has exchanged places with SrO no. 2, as depicted by the arrows in Fig. 1b. This interpretation was confirmed by quantitative fitting of the specular CTRs, revealing that the rearrangement happened either during or after growth of the $TiO_2$ layer such that

[1]X-ray Science Division, Argonne National Laboratory, Argonne, Illinois 60439, USA, [2]Department of Materials Science & Engineering, University of Wisconsin-Madison, 1509 University Avenue Madison, Wisconsin 53706, USA, [3]Department of Materials Science and Engineering, Northwestern University, Evanston, Illinois 60208, USA, [4]Materials Science Division, Argonne National Laboratory, Argonne, Illinois 60439, USA, [5]National Synchrotron Radiation Laboratory, University of Science and Technology of China, Hefei, Anhui 230026, China, [6]Chemical Sciences and Engineering Division, Argonne National Laboratory, Argonne, Illinois 60439, USA, [7]Center for Nanoscale Materials, Argonne National Laboratory, Argonne, Illinois 60439, USA, [8]Department of Materials Science & Engineering, and Institute of Materials Science, University of Connecticut, Storrs, Connecticut 06269, USA. †Present address: Neutron Science Division, Korea Atomic Energy Research Institute, Daejeon 305-600, Republic of Korea. ‡These authors contributed equally to this work. *e-mail: ddmorgan@wisc.edu; freeland@anl.gov

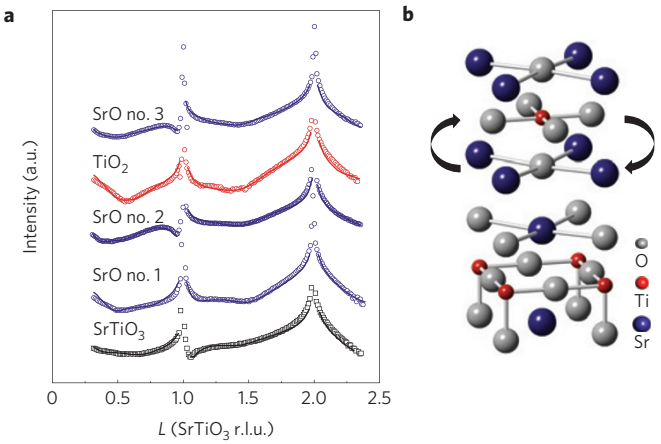


**Figure 1 | Layer swap during the growth of $Sr_2TiO_4$. a**, Scattered intensities along the 00*L* measured immediately after shuttered growth of each layer in the following sequence: SrO → SrO → $TiO_2$ → SrO (from bottom to top). The measured data are represented by symbols, and fitted intensities are represented by solid lines. **b**, The expected atomic structure of film based on the growth sequence and proposed layer swap that occurs in the real growth.

SrO → SrO → $TiO_2$ deposition forms the SrO–$TiO_2$–SrO structure. As seen from the time evolution of scattered intensity at the highly surface-sensitive anti-Bragg position (Supplementary Fig. 1), changes are observed only with the Ti shutter open, providing evidence that the exchange occurred during $TiO_2$ incorporation and is complete by the time 1 monolayer coverage of $TiO_2$ is reached.

To understand the energetic driving force for this layer rearrangement, we calculated and compared the energies of different stacking sequences using density functional theory[20,21] (DFT) as well as with the empirical modified Buckingham potential[22]. We first compared two structures comprised of the $TiO_2$-terminated $SrTiO_3$ substrate with two SrO layers and one $TiO_2$ layer, as shown in Fig. 2a,b. Relative to the intended SrO–SrO–$TiO_2$ structure, the SrO–$TiO_2$–SrO structure is more stable by ∼0.6 eV per Ti atom. This demonstrates that there is a significant thermodynamic driving force to rearrange the layers from SrO–SrO–$TiO_2$ to a SrO–$TiO_2$–SrO structure, in agreement with the exchange observed in Fig. 1. The good agreement between the DFT and empirical potential results shows that the physics captured by the latter, that is, short-range bonding and electrostatics, dominates the exchange energetics.

We then considered the effect of a third consecutive SrO layer in the stacking sequence, as shown in Fig. 2c. The SrO–SrO–$TiO_2$–SrO structure (Fig. 2d) was determined to be ∼1 eV per Ti atom more stable than SrO–SrO–SrO–$TiO_2$ and ∼0.4 eV per Ti atom more stable than SrO–$TiO_2$–SrO–SrO (Fig. 2e). $TiO_2$ will then exchange with the topmost SrO layer but not with the layer underneath. This result suggests that the immediate growth of the Ruddlesden–Popper phase can be accomplished by following the SrO → SrO → SrO → $TiO_2$ deposition sequence. We tested this hypothesis experimentally, again measuring the scattered intensity along the specular CTR after the growth of each layer. The final structure was SrO–SrO–$TiO_2$–SrO, as predicted, and continued growth of $Sr_2TiO_4$ can be accomplished by following the SrO → SrO → $TiO_2$ deposition sequence. Note that each $TiO_2$ layer will continue to exchange with the underlying SrO throughout the growth process, as the energetics for rearrangement change little as a function of film thickness (Supplementary Fig. 2a). Thus, only one extra SrO layer in the initial sequence is needed to stabilize the proper sequencing for the Ruddlesden–Popper phase.

Although rearrangement of the initial SrO–SrO–$TiO_2$ structure is energetically favourable, the atomic pathway by which the configuration change occurs is less clear. One possible path is that Ti can move directly into the SrO layer, with the displaced SrO species presumably diffusing on top of the forming $TiO_2$ plane during deposition. Although direct insertion into a SrO layer by an isolated $TiO_2$ is a high-energy process, with a 2.71 eV energy barrier, our DFT studies show that a $TiO_2$ molecule on the SrO bilayer attracts two neighbouring O atoms in the topmost SrO layer and forms a tetrahedral-like cluster, significantly disrupting the SrO layer and making it vulnerable to further attack (Supplementary Fig. 3). With two nearby $TiO_2$ molecules, the disruption can reduce the energy barrier to 1.18 eV (Supplementary Fig. 4), and in the presence of a Sr vacancy there is no barrier to $TiO_2$ incorporation, yielding a potentially rapid exchange process that can easily occur during the relatively slow $TiO_2$ deposition, especially given the presence of step edges, islands and defects that are connected to the synthesis of oxide thin films. Molecular dynamics simulations with partial coverage of $TiO_2$ show movement of Sr atoms close to the edge of the $TiO_2$ island from the underlayer to the surface, which is also consistent with role of defects as a pathway for layer swapping (Supplementary Fig. 5). Although the actual path that the system follows has not been observed directly, all of these mechanisms are consistent with our finding that the exchange is driven by $TiO_2$ layer deposition.

The results presented so far have been specific to strontium titanate Ruddlesden–Popper structures and $Sr_2TiO_4$ in particular; however, our calculations indicate that layer exchange is expected quite generally for different stoichiometries and materials systems. First, as shown in Fig. 3a, we illustrate that it is always energetically favourable for a $TiO_2$ surface layer to exchange with the underlying SrO layer without regard to the number of consecutive SrO layers. With this understanding, one can gain atomic-level control over the growth of any arbitrary $(SrO)_m(SrTiO_2)_n$ Ruddlesden–Popper sequence, as illustrated in Supplementary Fig. 2b. Among stackings of $(m\text{SrO})\text{TiO}_2(n\text{SrO})$, for $m+n>2$, the most stable configurations are the ones accompanied by at least two SrO planes underneath and at least one SrO plane above the $TiO_2$ (that is, $m \geq 2$ and $n \geq 1$). These energies are in accordance with the results of ref. 23, which reported that single $TiO_2$ planes surrounded by more than two consecutive SrO layers could be stabilized in a superlattice geometry even when the overall stoichiometry was not thermodynamically stable. Furthermore, we predict that layer rearrangement also occurs with other cations in the B-site, as shown in Fig. 3b. We considered seven other perovskite-forming B-site cations: V, Mn, Zr, Mo, Ru, Rh and Ir. These systems have cation radii ranging from ∼67 to ∼86 pm and different magnetic moments, but all show trends similar to those in the Ti system. Cations in the antiferromagnetic and non-magnetic states behaved similarly to those in the ferromagnetic state, suggesting that magnetism plays a minor role in driving the rearrangement (Supplementary Fig. 6a–c).

Detailed analyses of the strontium titanate system reveal that the driving force for layer exchange can be understood in terms of the cleavage energies (for example, energy to pull two surfaces apart) of three relevant interfaces, which are largely independent of the surrounding environment. These interfaces are S/S, T/ST and T/SS, where S, T and / represent the SrO plane, the $TiO_2$ plane and the interface, respectively. As elucidated in the Supplementary Information, the energy differences of different stackings can be quantitatively modelled by cleavage energy differences (Supplementary Fig. 7). The cleavage energies of the three interfaces are ordered as S/S (∼1.34 eV) <T/ST (∼2.17 eV) <T/SS (∼2.62 eV). This ordering is intuitive: the S/S interface is less stable than the T/ST interface because it contains fewer chemical bonds per unit area, and the T/SS interface is more stable than that for T/ST, owing to weaker bonding in the adjacent SS

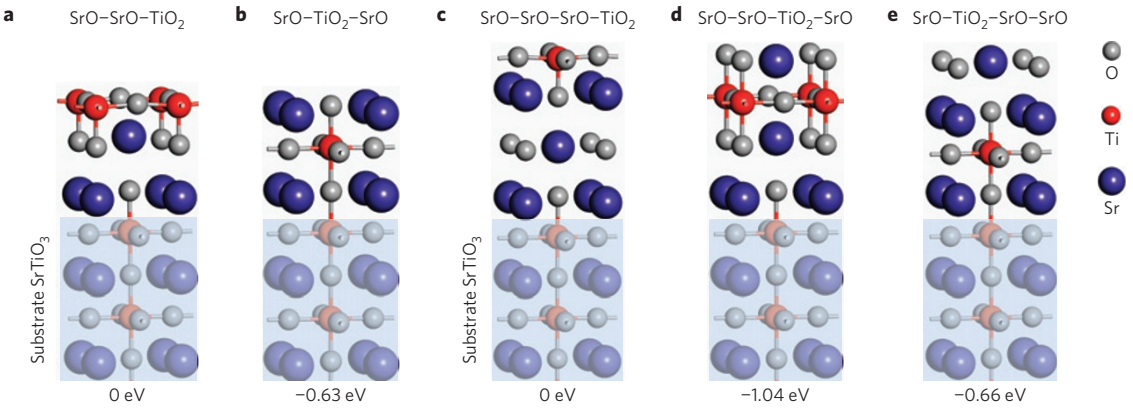


**Figure 2 | Energetics for different layer sequencing during growth. a–e**, Optimized structures and relative energies of different stackings of two (**a**,**b**) or three (**c**–**e**) SrO and one $TiO_2$ layer on a $TiO_2$-terminated $SrTiO_3$ substrate. Stackings are labelled by their layers from the first layer above the substrate surface to the top interface with vacuum. All relative energies are measured per unit cell and have the unit of electronvolts per exchanged Ti atom. Part of the substrate is indicated by shaded areas to guide the eyes.

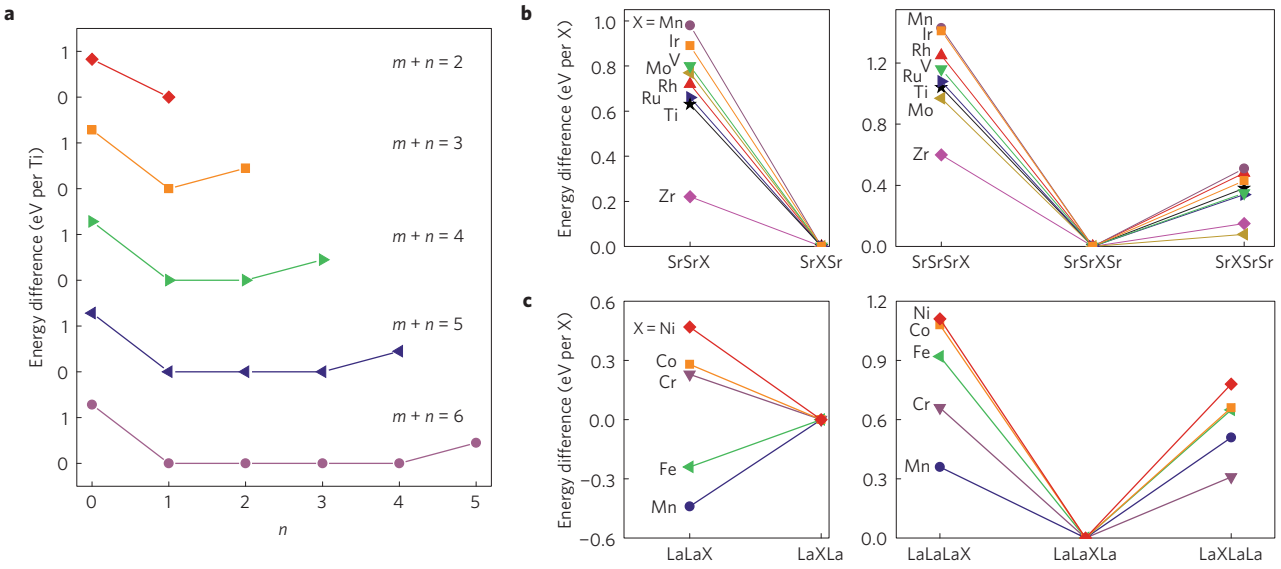


**Figure 3 | Layer swapping in additional systems. a**, Energy differences among stackings of ($TiO_2$-terminated substrate)-($m$SrO)$TiO_2$($n$SrO) for $m+n=2,3,4,5,6$. For simple stacking notation, hereafter, we leave out the substrate and the O in an oxide layer. Thus, the ($TiO_2$-terminated substrate)-($m$SrO)$TiO_2$($n$SrO) is written as ($m$Sr)Ti($n$Sr). **b**, Energy differences among stackings of ($m$Sr)X($n$Sr) at $m+n=2$ and 3 for X = Ti, V, Mn, Zr, Mo, Ru, Rh and Ir in the B-site. **c**, Energy differences among stackings of ($m$La)X($n$La) at $m+n=2$ and 3 for X = Cr, Mn, Fe, Co and Ni in the B-site. All calculations for magnetic systems are done with ferromagnetic ordering.

bilayer. Such energy ordering drives layer rearrangement to form more locally stable interfaces in place of less stable ones. Using the above-mentioned three cleavage energies in our model, we can accurately reproduce the DFT results in Fig. 3a, as shown in Supplementary Fig. 8.

Finally, we considered whether layer rearrangement is unique to strontium-based systems or can take place in other materials grown on $SrTiO_3$, such as the lanthanum-based transition-metal oxides, $La_{n+1}B_nO_{3n+1}$. The La-based materials differ substantially from those of the strontium-based oxides in that the (001) planes are nominally polar[24], in contrast to the mostly charge-neutral planes in strontium systems. As observed in Fig. 3c, layer rearrangement is again expected to occur for many B-site cations. The exchange will always take place on LaO trilayers, regardless of the magnetic state. We do find, however, that the LaO–LaO–Mn and LaO–LaO–Fe structures are stable, whenever Mn or Fe are in the ferromagnetic or antiferromagnetic state, which may originate from large magnetic interactions (Supplementary Fig. 6d–f).

To illustrate how our insight can provide a pathway to stabilize new phases and to confirm our predictions, we conducted a set of *in situ* growth experiments for $(LaO)(LaNiO_3)_n$ similar to those for the strontium titanates. We used a growth temperature of 600 °C and employed ozone as the oxidant. As predicted in Fig. 3c, layer rearrangement was indeed observed, and the same strategy for producing $Sr_2TiO_4$ was used to grow both $La_2NiO_4$ and $La_3Ni_2O_7$. The $La_3Ni_2O_7$ structure was obtained by following the deposition sequence LaO → LaO → LaO → $NiO_2$ → $NiO_2$, which, after the predicted layer exchange, results in LaO–LaO–$NiO_2$–LaO–$NiO_2$ ordering. Note that by combining the shuttered growth technique with this strategy, one achieves a level of control over cation ordering greater than that of direct transfer from stoichiometric target[25]. The specular CTR from a film grown by six repeats of that sequence is shown as the red curve in Fig. 4a, and its corresponding X-ray absorption spectroscopy (XAS) profile measured at the Ni *L*-edge is shown in Fig. 4b. The specular CTR exhibits strong thickness fringes and Bragg peaks, indicating sharp interfaces and

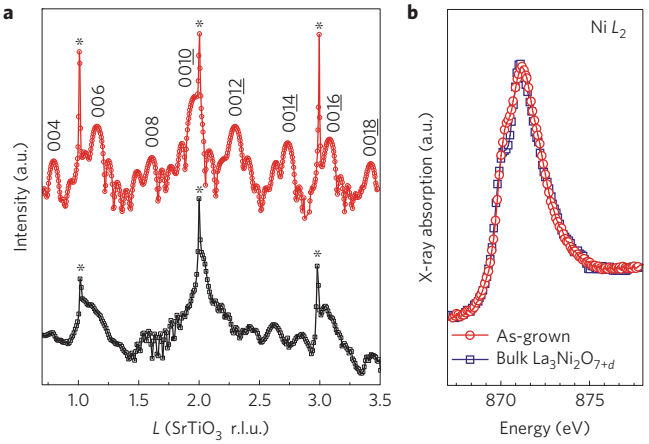


**Figure 4 | Synthesis of single-crystal $La_3Ni_2O_7$. a**, Specular crystal truncation rods for a film grown with the LaO → LaO → LaO → $NiO_2$ → $NiO_2$ sequence (red) and for film grown using the LaO → LaO → $NiO_2$ → LaO → $NiO_2$ sequence (black). Peaks from the substrate are indicated with asterisks. **b**, X-ray absorption spectroscopy spectra for the $La_3Ni_2O_7$ film (red) and a powder sample (blue).

high crystalline quality. For comparison, a sample grown with the LaO → LaO → $NiO_2$ → LaO → $NiO_2$ sequence is shown in black. There are no signs of the $La_3Ni_2O_7$ Bragg peaks, and the scattered intensity exhibits signatures of a highly defective film. The XAS spectrum in Fig. 4b is compared to that from a $La_3Ni_2O_{7-\delta}$ powder[26], where $\delta$ is 0 ±0.02, as determined by thermogravimetric analysis, illustrating that the nickel valence has the expected value of ∼2.5+.

The synthesis methodology used here, coupling quantitative *in situ* X-ray scattering with computational theory, is an approach that can be readily extended to other layered materials and heterostructures. Of particular interest are those predicted to exhibit new properties but have yet to synthesized owing to various growth challenges, such as the polar $PbSr_2Ti_2O_7$ (ref. 27) or many of the layered oxides described in refs 28–31. One is not limited to simply layered oxides and can use this approach to explore wholly new oxide archetypes that have yet to be synthesized as thin-film heterostructures. We find the insights garnered when *in situ* X-ray results are fed back to computational theory to be of considerable importance as they allow the rapid formulation of growth strategies that may be critical to the material, even for deposition techniques as precise as MBE. This close integration with computational theory is an aspect of synthesis science that will become more essential as we create new materials by design and rapidly seek pathways to stabilize new phases.

## Methods

Films were grown in the *in situ* X-ray chamber at Sector 33ID-E of the APS using molecular beam epitaxy. The $(SrO)(SrTiO_3)_n$ films were grown at 750 °C and in $10^{-6}$ Torr of $O_2$ using a Sr effusion cell and a Ti-Ball source. Grow rates ranged from 1 to 3 min per monolayer depending on the species.

We performed *ab initio* calculations using DFT, as coded in the Vienna *ab initio* simulation package[20,21]. We chose the PBEsol functional[32], which was demonstrated to be excellent for the description of bulk $SrTiO_3$ (ref. 33). The projector augmented wave method is used with the following potentials for $SrTiO_3$:O ($2s^22p^4$, $E_{cut}$ = 400.0 eV), Ti ($3p^63d^{10}4s^2$, $E_{cut}$ = 274.6 eV) and Sr ($4s^24p^65s^2$, $E_{cut}$ = 229.3 eV). The plane-wave energy cutoff is set to 500 eV. We approximate the substrate with 20 atomic layers (∼3.7 nm) of cubic $SrTiO_3$, with the bottom 10 atomic layers fixed to the optimized bulk positions and the other layers relaxed. To reduce the mirror interactions between neighbouring supercells, we add a vacuum slab as thick as 1.5 nm and consider dipole corrections in the out-of-plane direction. The supercells in the plane are one or two unit cell sizes large and the Monkhorst–Pack *k*-point grids for Brillouin zone sampling are 6 × 6 × 1 and 4 × 4 × 1, respectively.

The functional form and parameters of the empirical Buckingham potential[22] used in structural optimizations and molecular dynamics simulations are given in the Supplementary Information. The optimizations are performed using gradient-based techniques. The convergence criteria for energy and interatomic distances are 0.001 eV and 0.0005 Å, respectively. The molecular dynamics runs are carried out with the Verlet propagator and a step size of 5 fs. A Nosé type thermostat, as implemented in the DL_POLY software package, is used to control the temperature.

Received 11 February 2014; accepted 19 June 2014; published online 3 August 2014

## References


1. Bibes, M., Villegas, J. & Barthelemy, A. Ultrathin oxide films and interfaces for electronics and spintronics. *Adv. Phys.* **60,** 5–84 (2011).
2. Chakhalian, J., Millis, A. J. & Rondinelli, J. Whither the oxide interface. *Nature Mater.* **11,** 92–94 (2012).
3. Rondinelli, J. M., May, S. J. & Freeland, J. W. Control of octahedral connectivity in perovskite oxide heterostructures: An emerging route to multifunctional materials discovery. *Mater. Res. Soc. Bull.* **37,** 261–270 (2012).
4. Eckstein, J. N. & Bozovic, I. High-temperature superconducting multilayers and heterostructures grown by atomic layer-by-layer molecular beam epitaxy. *Annu. Rev. Mater. Sci.* **25,** 679–709 (1995).
5. Yamamoto, H., Naito, M. & Sato, H. A new superconducting cuprate prepared by low-temperature thin-film synthesis in a Ba–Cu–O system. *Jpn. J. Appl. Phys.* **36,** L341–L344 (1997).
6. Schlom, D. G., Chen, L-Q., Pan, X., Schmehl, A. & Zurbuchen, M. A. A Thin film approach to engineering functionality into oxides. *J. Am. Ceram. Soc.* **91,** 2429–2454 (2008).
7. Locquet, J. P., Catana, A., Mächler, E., Gerber, J. & Bednorz, J. G. Block-by-block deposition: A new growth method for complex oxide thin films. *Appl. Phys. Lett.* **64,** 372–374 (1994).
8. Ruddlesden, S. N. & Popper, P. New compounds of the $K_2NiF_4$ type. *Acta Crystallogr.* **10,** 538–539 (1957).
9. Haeni, J. H. *et al.* Epitaxial growth of the first five members of the $Sr_{n+1}Ti_nO_{3n+1}$ Ruddlesden–Popper homologous series. *Appl. Phys. Lett.* **78,** 3292–3294 (2001).
10. Lee, C-H. *et al.* Effect of reduced dimensionality on the optical band gap of $SrTiO_3$. *Appl. Phys. Lett.* **102,** 122901 (2013).
11. Udayakumar, K. R. & Cormack, A. N. Structural aspects of phase equilibria in the strontium–titanium–oxygen system. *J. Am. Ceram. Soc.* **71,** C469–C471 (1988).
12. Noguera, C. Theoretical investigation of the Ruddlesden–Popper compounds $Sr_{n+1}Ti_nO_{3n+1}$ ($n = 1-3$). *Phil. Mag. Lett.* **80,** 173–180 (2000).
13. Le Bacq, O., Salinas, E., Pisch, A., Bernard, C. & Pasturel, A. First-principles structural stability in the strontium–titanium–oxygen system. *Phil. Mag.* **86,** 2283–2292 (2006).
14. McCoy, M. A., Grimes, R. W. & Lee, W. E. Phase stability and interfacial structures in the SrO–$SrTiO_3$ system. *Phil. Mag. A* **75,** 833–846 (1997).
15. Tian, W., Pan, X. Q., Haeni, J. H. & Schlom, D. G. Transmission electron microscopy study of $n = 1-5Sr_{n+1}Ti_nO_{3n+1}$ epitaxial thin films. *J. Mater. Res.* **16,** 2013–2026 (2001).
16. Lee, C-H. *et al.* Exploiting dimensionality and defect mitigation to create tunable microwave dielectrics. *Nature* **502,** 532–536 (2014).
17. Koster, G., Kropman, B. L., Rijnders, G. J. H. M., Blank, D. H. A. & Rogalla, H. Quasi-ideal strontium titanate crystal surfaces through formation of strontium hydroxide. *Appl. Phys. Lett.* **73,** 2920–2922 (1998).
18. Nie, Y. F. *et al.* Atomically precise interfaces from non-stoichiometric deposition. *Nature Commun.* **5,** 4530 (2014).
19. Hong, H. & Chiang, T-C. A six-circle diffractometer system for synchrotron X-ray studies of surfaces and thin film growth by molecular beam epitaxy. *Nucl. Instrum. Methods Phys. Res. A* **572,** 942–947 (2007).
20. Kresse, G. & Furthmuäller, J. Efficient iterative schemes for *ab initio* total-energy calculations using a plane-wave basis set. *Phys. Rev. B* **54,** 11169–11186 (1996).
21. Kresse, G. & Furthmuäller, J. Efficiency of *ab-initio* total energy calculations for metals and semiconductors using a plane-wave basis set. *Comput. Mater. Sci.* **6,** 15–50 (1996).
22. Sekiguchi, S. *et al.* Atomic force microscopic observation of $SrTiO_3$ polar surface. *Solid State Ion.* **108,** 73–79 (1998).
23. Fisher, P. *et al.* A series of layered intergrowth phases grown by molecular beam epitaxy: $Sr_mTiO_{2+m}$ ($m = 1-5$). *Appl. Phys. Lett.* **91,** 252901 (2007).
24. Goniakowski, J., Finocchi, F. & Noguera, C. Polarity of oxide surfaces and nanostructures. *Rep. Prog. Phys.* **71,** 016501 (2008).
25. Wu, K-T., Soh, Y-A. & Skinner, S. J. Epitaxial growth of mixed conducting layered Ruddlesden–Popper $La_{n+1}Ni_nO_{3n+1}$ ($n = 1$, 2 and 3) phases by pulsed laser deposition. *Mater. Res. Bull.* **48,** 3783–3789 (2013).
26. Zhang, Z., Greenblatt, M. & Goodenough, J. Synthesis, structure, and properties of the layered perovskite $La_3Ni_2O_7$-δ. *J. Solid State Chem.* **108,** 402 (1994).

27. Nakhmanson, S. M. & Naumov, I. Goldstone-like states in a layered perovskite with frustrated polarization: A first-principles investigation of $PbSr_2Ti_2O_7$. *Phys. Rev. Lett.* **104,** 097601 (2010).
28. Benedek, N. & Fennie, C. Hybrid improper ferroelectricity: A mechanism for controllable polarization–magnetization coupling. *Phys. Rev. Lett.* **106,** 107204 (2011).
29. Birol, T., Benedek, N. A. & Fennie, C. J. Interface control of emergent ferroic order in Ruddlesden–Popper $Sr_{n+1}Ti_nO_{3n+1}$. *Phys. Rev. Lett.* **107,** 257602 (2011).
30. Rondinelli, J. M. & Fennie, C. J. Octahedral rotation-induced ferroelectricity in cation ordered perovskites. *Adv. Mater.* **24,** 1961–1968 (2012).
31. Mulder, A. T., Benedek, N. A., Rondinelli, J. M. & Fennie, C. J. Turning $ABO_3$ antiferroelectrics into ferroelectrics: Design rules for practical rotation-driven ferroelectricity in double perovskites and $A_3B_2O_7$ Ruddlesden-Popper compounds. *Adv. Funct. Mater.* **23,** 4810–4820 (2013).
32. Perdew, J. *et al.* Restoring the density-gradient expansion for exchange in solids and surfaces. *Phys. Rev. Lett.* **100,** 136406 (2008).
33. Wahl, R., Vogtenhuber, D. & Kresse, G. $SrTiO_3$ and $BaTiO_3$ revisited using the projector augmented wave method: Performance of hybrid and semilocal functionals. *Phys. Rev. B* **78,** 104116 (2008).

## Acknowledgements

The authors acknowledge discussions with D. G. Schlom, K. Lee and Y. Nie, and support at the APS from H. Zhou and C. Schlepütz. S.H.C., J.A.E., A.B. and D.D.F. were supported by the US. Department of Energy, Office of Science, Materials Sciences and Engineering Division. Work performed at Argonne National Laboratory, including the Advanced Photon Source, was supported by the US Department of Energy, Office of Science, Office of Basic Energy Sciences, under contract no. DE-AC02-06CH11357. The calculations were carried out on the Fusion Cluster of Argonne's Laboratory Computing Resource Center, at NERSC (supported by DOE), and on Argonne's Carbon Cluster under award CNM29783 and CNM35702. D.M. and G.L. were partially supported by University of Wisconsin Materials Research Science and Engineering Center (DMR-1121288).

## Author contributions

J.H.L., Z.L., I.C.T., S.H.C., A.B., J.A.E., H.H., D.D.F. and J.W.F. developed the *in situ* oxide MBE system and participated in the real-time growth experiments. J.H.L., Z.L., I.C.T., D.D.F. and J.W.F. handled analysis of the experimental data. G.L., M.M., M.G., S.M.N., J.J. and D.M. were responsible for the detailed theoretical calculations related to the experiments. All authors participated in the discussion of data/analysis/conclusions and in the writing of the manuscript.

## Additional information

Supplementary information is available in the online version of the paper. Reprints and permissions information is available online at www.nature.com/reprints. Correspondence and requests for materials should be addressed to D.M. or J.W.F.

## Competing financial interests

The authors declare no competing financial interests.